Key Points:
- Consistent and robust 10 year comparison of MODIS and model urban LST
- Specifying urban fraction in each pixel improves simulated temperature
- Irrigating urban vegetated areas reduces model biases and improves precision

Correspondence to:
A. J. Monaghan,
monaghan@ucar.edu

Evaluating the impact of urban morphology configurations on the accuracy of urban canopy model temperature simulations with MODIS

Andrew J. Monaghan[1], Leiqiu Hu[2], Nathaniel A. Brunsell[2], Michael Barlage[1], and Olga V. Wilhelmi[1]

[1]National Center for Atmospheric Research, Boulder, Colorado, USA, [2]Department of Geography, University of Kansas, Lawrence, Kansas, USA

Abstract Simulations of the urban environment contribute to assessments of current and future urban vulnerabilities to extreme heat events. The accuracy of simulations of the urban canopy can be degraded by inaccurate or oversimplified representations of the urban-built environment within models. Using a 10 year (2003–2012) series of offline 1 km simulations over Greater Houston with the High-Resolution Land Data Assimilation System (HRLDAS), this study explores the model accuracy gained by progressively increasing the complexity of the urban morphology representation in an urban canopy model. The fidelity of the simulations is primarily assessed by a spatiotemporally consistent comparison of a newly developed HRLDAS radiative temperature variable with remotely sensed estimates of land surface temperature from the Moderate Resolution Imaging Spectroradiometer. The most accurate urban simulations of radiative temperature are yielded from experiments that (1) explicitly specify the urban fraction in each pixel and (2) include irrigation. The former modification yields a gain in accuracy that is larger than for other changes, such as increasing the number of urban land use types. The latter modification (irrigation) substantially reduces simulated temperature biases and increases model precision compared to model configurations that lack irrigation, presumably because watering of lawns, parks, etc. is a common activity that should be represented in urban canopy models (although it is generally not). Ongoing and future efforts to improve urban canopy model simulations may achieve important gains through better representations of urban morphology, as well as processes that affect near-surface energy partitioning within cities, such as irrigation.

1. Introduction

Extreme heat events are a leading cause of weather-related human mortality in the United States [*Centers for Disease Control and Prevention*, 2006; *Borden and Cutter*, 2008]. The impact of extreme heat events on urban populations is particularly acute [e.g., *Curriero et al.*, 2002], in part because cities are generally warmer than adjacent rural areas due to the characteristics of the built environment [*Oke et al.*, 1991; *Li and Bou-Zeid*, 2013]. Extreme heat events disproportionally impact the most vulnerable groups within cities, including the elderly, minorities, linguistically and socially isolated persons, low income groups, and those with preexisting medical conditions [*Schuman*, 1972; *Jones et al.*, 1982; *Semenza et al.*, 1996; *Medina-Ramon et al.*, 2006; *Uejio et al.*, 2011]. Previously rare extreme heat events are now occurring with increased frequency and intensity in some regions of the United States, and are projected to become common throughout the country in the 21st century, partly due to greater persistence of weather patterns that cause them [*Duffy and Tebaldi*, 2012; *Diffenbaugh and Ashfaq*, 2010; *Meehl and Tebaldi*, 2004]. As a result, heat-related mortality is projected to rise [*Patz et al.*, 2000, 2005; *Greene et al.*, 2011].

The System for Integrated Modeling of Metropolitan Extreme Heat Risk (SIMMER) is a project funded by the National Aeronautics and Space Administration (NASA) to comprehensively characterize and address urban extreme heat risk. The objectives of SIMMER are to advance methodologies for assessing current and future urban vulnerabilities to extreme heat events through the refinement and integration of physical and social science models [*Wilhelmi and Hayden*, 2010; *Heaton et al.*, 2014] and to build local capacity for heat hazard mitigation and climate change adaptation in the public health sector. SIMMER is being developed and tested over Greater Houston, Texas (Figure 1a), due to its warm and humid
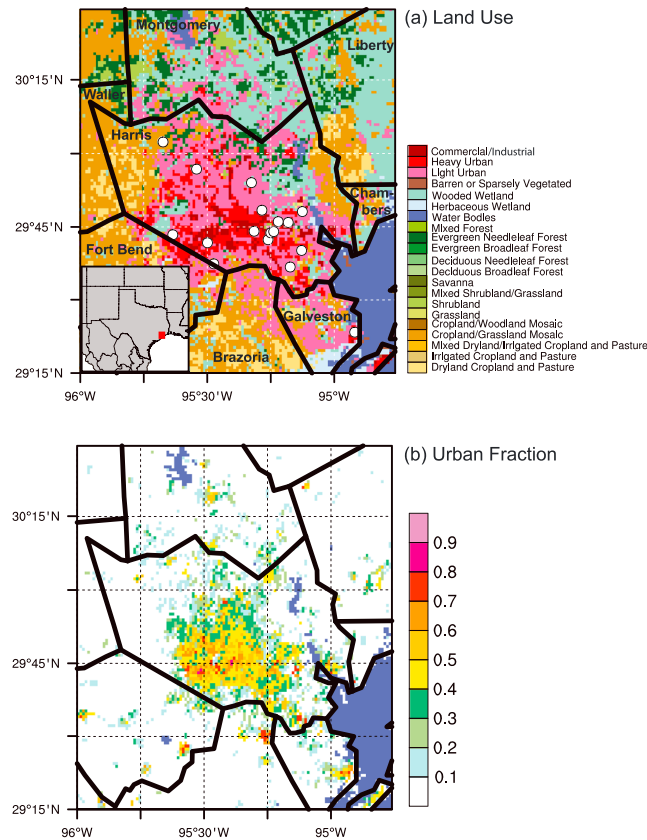
Figure 1. (a) HRLDAS 0.01° model domain over the Greater Houston area showing the land use type for each grid box (counties indicated in black font). The three urban land use types are defined from NLCD. Locations of TEXAQS-II weather stations used for model validation are indicated by white circles. A regional inset map showing the location of Greater Houston (red box) is included in the lower left corner. (b) Fraction of each grid box that is specified as any category of urban in NUDAPT. Dark blue areas denote water bodies.

subtropical climate that is characterized by extreme heat events in the warm season that are projected to become more frequent in the future [e.g., *Oleson et al.*, 2013]. The present study investigates how the characterization of urban morphology within an urban canopy model (UCM) can impact the accuracy of simulations of near-surface temperature in Greater Houston.

Approaches for modeling the urban canopy range from "slab" routines that treat the urban area as a homogeneous, yet distinct region [e.g., *Atwater*, 1972], to single-layer UCMs that treat a simplified urban canyon geometry below a specified level of near-surface atmospheric forcing [e.g., *Mills*, 1997; *Masson*, 2000; *Kusaka et al.*, 2001], to multilayer UCMs in which the urban canopy projects upward into the lowest several layers of forcing within an atmospheric model [*Kondo and Liu*, 1998; *Vu et al.*, 1999]. Generally speaking, urban meteorology is better simulated when using single-level and multilevel UCMs as opposed to slab treatments, when land use properties are explicitly defined instead of parameterized, and when the UCM—usually embedded within a land surface model (LSM)—is coupled to an atmospheric model and the models are integrated

simultaneously [e.g., *Kusaka and Kimura*, 2004; *Kusaka et al.*, 2004, 2012a, 2012b; *Otte et al.*, 2004; *Best*, 2005; *Chen et al.*, 2011a; *Miao et al.*, 2011; *Salamanca et al.*, 2011]. The coupled approach allows adjacent urban and rural grid cells to interact via advection of state variables within the atmospheric model [e.g., *Freitas et al.*, 2007; *Dandou et al.*, 2009].

Numerous studies have employed UCMs coupled to atmospheric models to investigate the urban meteorology of Houston. The results indicate that the built environment of Houston has important influences on the spatial and temporal variability of near-surface air temperatures [*Kusaka et al.*, 2004; *Salamanca et al.*, 2011], the timing and magnitude of sea breezes [*Bornstein et al.*, 2006; *Chen et al.*, 2011b; *Carter et al.*, 2012], and the spatial distribution, frequency, and intensity of rainfall [*Shepherd et al.*, 2010]. The results of these papers also suggest that model deficiencies are partly linked to inaccurate or oversimplified representations of the urban-built environment within UCMs [e.g., *Cheng and Byun*, 2008], thus motivating the present work. Using a series of 1 km simulations over Greater Houston, this study explores the model accuracy gained by progressively increasing the complexity of the urban morphology representation in a UCM. The fidelity of the simulations is assessed via comparison to in situ observations of air temperature and remotely sensed estimates of land surface temperature (LST) from the Moderate Resolution Imaging Spectroradiometer (MODIS) onboard NASA's Terra and Aqua satellites. A particularly novel aspect of the work is the use of a rigorously tested methodology for comparison of the simulations to the MODIS LST, developed by *Hu et al.* [2014]. Methods are described in section 2, results presented in section 3, and discussion and conclusions provided in section 4.

Table 1. Parameter Values Employed in the HRLDAS UCM for Each Urban Surface Type (Light-Intensity Urban = LU, Heavy-Intensity Urban = HU, Commercial/Industrial-Intensity Urban = CU)

Parameter	LU	HU	CU	Units	HRLDAS Name
Urban fraction[a]	0.50	0.90	0.95	-	FRC_URB
Exchange coefficient[b]	0.30	0.40	0.50	-	AKANDA_URBAN
Building height	5.0	7.5	10.0	m	ZR
Roof width	8.3	9.4	10.0	m	ROOF_WIDTH
Road width	8.3	8.4	10.0	m	ROAD_WIDTH
Roof heat capacity	1.0E+06	1.0E+06	1.0E+06	$J\,m^{-3}\,K^{-1}$	CAPR
Wall heat capacity	1.0E+06	1.0E+06	1.0E+06	$J\,m^{-3}\,K^{-1}$	CAPB
Road heat capacity	1.4E+06	1.4E+06	1.4E+06	$J\,m^{-3}\,K^{-1}$	CAPG
Roof conductivity	0.67	0.67	0.67	$J\,m^{-1}\,s^{-1}\,K^{-1}$	AKSR
Wall conductivity	0.67	0.67	0.67	$J\,m^{-1}\,s^{-1}\,K^{-1}$	AKSB
Road conductivity	0.4004	0.4004	0.4004	$J\,m^{-1}\,s^{-1}\,K^{-1}$	AKSG
Roof albedo	0.20	0.20	0.20	-	ALBR
Wall albedo[b]	0.40	0.40	0.40	-	ALBB
Road albedo[b]	0.30	0.30	0.30	-	ALBG
Roof emissivity	0.90	0.90	0.90	-	EPSR
Wall emissivity	0.90	0.90	0.90	-	EPSB
Road emissivity	0.95	0.95	0.95	-	EPSG
Roof roughness length	0.01	0.01	0.01	m	Z0R
Wall roughness length	0.0001	0.0001	0.0001	m	Z0B
Road roughness length	0.01	0.01	0.01	m	Z0G

[a]Values for experiments A1/A2, B1/B2, and C1/C2. Spatially explicit values used for experiments D1/D2.
[b]Modified from default values.

2. Methodology

2.1. Modeling

2.1.1. Overview

The meteorology of Houston's urban heat island (UHI) is simulated using an offline version of the Noah Land Surface Model (Noah LSM) [e.g., *Chen and Dudhia*, 2001], known as the High-Resolution Land Data Assimilation System (HRLDAS) [*Chen et al.*, 2007]. The Noah LSM simulates the fluxes of energy and water from the land surface as a function of the underlying land surface and soil properties while also maintaining stores of water and energy in four soil layers to a depth of 2 m. The offline HRLDAS framework is chosen as opposed to performing "online" coupled WRF-Noah LSM simulations, because the former approach is 1 to 2 orders of magnitude less expensive computationally, an important consideration because of the number of long-term (10 year) high-resolution (1 km) simulations required. While the offline approach neglects the coupled atmosphere-land surface interactions that are important in Houston, such as sea breezes [e.g., *Chen et al.*, 2011b], it is well suited for the objectives of the present work, as will be demonstrated in the results section.

In order to better represent the physical processes involved in the exchange of heat, momentum, and water vapor in the urban environment, a UCM [*Kusaka et al.*, 2001] is coupled to the Noah LSM [*Chen et al.*, 2004; *Kusaka et al.*, 2004]. The main purpose of the coupled model is to improve the description of the lower boundary conditions and to provide more accurate simulations for urban regions. The UCM is a single layer model with simplified urban geometry. Features of the UCM include shadowing from buildings, diurnal changes of the solar azimuth angle, reflection of short- and long-wave radiation, and multilayer heat transfer equations for roof, wall, and road surfaces [*Kusaka and Kimura*, 2004].

2.1.2. Modifications for This Study

It is necessary to estimate heat transfer from the natural surface (parks, recreation areas, etc.) when a grid cell is not fully covered by urban "artificial" surface. Therefore, the UCM is coupled to the Noah LSM through an "urban fraction" parameter to represent urban subgrid-scale heterogeneity. The urban land use categories for Houston are estimated from the 30 m resolution 2001 U.S. Geological Survey National Land Cover Database (NLCD 2001) [*Homer et al.*, 2004]. The urban surface has three categories: (1) light intensity, (2) heavy intensity, and (3) commercial/industrial usage (Figure 1a). Each category has unique parameters such as albedo, emissivity, heat capacity, roughness, and urban fraction that distinguish the urban environments from each other and from the outlying rural areas (Table 1). The urban fraction parameter is prescribed in some experiments (described below) explicitly using the National Urban Database and Access Portal Tool

(NUDAPT) [*Ching et al.*, 2009; *Burian and Ching*, 2009], a two-dimensional data set of critical urban properties (Figure 1b). The use of NUDAPT provides a more heterogeneous and realistic UHI characterization for the HRLDAS simulations compared to using the one-dimensional lookup table values for each urban category. Other minor modifications applied to all three urban types include (1) increasing the broadband albedo (reflectivity) of road surfaces from 0.2 to 0.3 and wall surfaces from 0.2 to 0.4 to more accurately characterize the pavement and buildings typical of Houston and (2) modifying the parameters used in the *Kanda et al.* [2007] approach for calculating the urban canopy exchange coefficients, so as to simulate more vigorous (and realistic) sensible heat exchanges between the urban canopy and atmosphere aloft (variable AKANDA_URBAN in URBPARM.TBL is changed to 0.5, 0.4, and 0.3 from 1.29, 1.29, and 1.29).

2.1.3. HRLDAS Output

Half-hourly, 1 km resolution HRLDAS simulations are performed over metropolitan Houston for 2003–2012, preceded by a 1 year (2002) "spin-up" period to allow the soil temperature and moisture states to equilibrate. The upper boundary conditions for HRLDAS are derived from one-eighth degree hourly meteorological data from the North American Land Data Assimilation Phase 2 (NLDAS-2) [*Cosgrove et al.*, 2003; *Xia et al.*, 2012] forcing data set. NLDAS-2 was originally developed to provide a high-quality, long-term data set to drive a suite of research-grade land-surface models [*Cosgrove et al.*, 2003; *Mitchell et al.*, 2004] but has subsequently been used for a variety of climate research applications over central North America. The nonprecipitation fields in the NLDAS-2 forcing data are derived from analysis fields of the National Centers for Environmental Prediction (NCEP) North American Regional Reanalysis (NARR) [*Mesinger et al.*, 2006] with bias corrections for downward solar radiation using satellite data from the National Environmental Satellite, Data, and Information Service Geostationary Satellite system. A vertical adjustment is applied to the fields of surface pressure, surface-downwelling long-wave radiation, near-surface air temperature and near-surface specific humidity to account for the vertical difference between the NARR and NLDAS-2 topographic height. The precipitation field is developed from a temporal disaggregation of a gauge-only analysis of daily precipitation from the NCEP Climate Prediction Center, augmented with satellite- and radar-derived precipitation estimates. The forcing level height of NLDAS-2 over Greater Houston varies from approximately 25–40 m above ground level (AGL), generally well above the urban canopy. The NLDAS-2 data are interpolated to the 1 km HRLDAS domain and smoothed before forcing the simulations.

Output for the June–August (JJA) summer months from the half-hourly HRLDAS simulations are used to calculate diagnostic surface radiative temperature (T_{rad}) and 2 m AGL air temperature (T_{air}) variables for use in the present study, in order to ensure that the simulated fields are as similar as possible to the observational fields they are validated against, which are described below. HRLDAS T_{rad}, which would be considered at nadir if viewed from space, is calculated as follows. At each time step, the energy balances for the roof, wall, and road components for each grid cell-containing urban areas are simulated by the UCM subroutine within the Noah LSM. The simulated outward long-wave radiation values for the roof, wall, and road are then combined into a bulk urban long-wave radiation value for each grid cell, based on the weighted average of the roof and canyon (considering sky-view geometry for the wall and road) long-wave radiation components. A bulk urban emissivity value is calculated in the same manner for each grid cell. Concurrently, the long-wave radiation is calculated in the LSM for the vegetated portion of each grid cell. Then, the bulk urban and vegetated long-wave radiation and emissivity values are averaged, weighted by their fractional area in each grid cell. Finally, these resulting "integrated" long-wave radiation and emissivity values for each grid cell are used to calculate T_{rad} using the Stefan-Boltzmann law. The component radiative temperatures for the vegetated and urban portions of each grid cell (T_{rad_V} and T_{rad_U}), as well as the roof, wall, and road areas comprising the urban portions (T_{roof}, T_{wall}, and T_{road}) are employed for additional in-depth analysis, being calculated from their respective component long-wave radiation and emissivity values.

T_{air} is calculated as follows. For the vegetated portion of each grid cell, T_{air} is calculated as a departure from the surface skin temperature based on the sensible heat flux and the atmospheric stability, manifested as an exchange parameter calculated at 2 m AGL following heat transfer theory [*Arya*, 1998]. In grid cells containing urban areas, the vegetation type is uniformly set to savanna, (i.e., a blend of grass and trees), the default urban vegetation type for the UCM. For the urban portion of the grid cell, T_{air} is approximated by the simulated urban canopy air temperature, which is a function of the sensible heat- and long-wave radiative fluxes from the canyon walls and road (air temperature over urban surfaces cannot be calculated using skin temperature as it is for vegetated surfaces, because urban skin temperature in the Noah LSM is calculated at the top of the

Table 2. List of HRLDAS Simulation Experiments

Experiment	Description	# Urban Categories	NUDAPT?	Irrigated?
A1	Vegetation only	0	No	No
B1	One-category urban	1	No	No
C1	Three-category urban	3	No	No
D1	Three-category urban with NUDAPT	3	Yes	No
A2	Same as A1 but irrigated	0	No	Yes
B2	Same as B1 but irrigated	1	No	Yes
C2	Same as C1 but irrigated	3	No	Yes
D2	Same as D1 but irrigated	3	Yes	Yes

canyon rather than within it). Finally, T_{air} for the entire grid cell is calculated as the area-weighted average of the cell's vegetated and urban components of T_{air}.

2.1.4. HRLDAS Experiments

Eight experiments are performed in which the complexity of the urban land use representation within simulations is progressively increased (Table 2). Experiment A1 is a vegetation-only experiment in which it is assumed that all grid cells containing urban areas are 100% vegetated with the urban default "savanna" vegetation type. Experiment B1 employs the "default" one-category urban land use type in HRLDAS, which involves setting all urban grid cells to the light-intensity urban type. The urban fraction of each grid cell containing any urban area is specified by the UCM default value of 0.5. Experiment C1 employs the three-category urban land use types specified by NLCD, as described above, with the urban fraction being specified as 0.5, 0.90, and 0.95 respectively for all light-intensity, heavy-intensity, and commercial/industrial grid cells. Experiment D1 is the same as C1, except that the urban fraction of each grid cell is specified explicitly by NUDAPT. Experiments A2–D2 are identical to A1–D1, except that it is assumed all vegetated surfaces are irrigated/watered. This is achieved by not allowing the volumetric soil moisture in any of the four soil layers to fall below 0.3. All experiments use the same urban footprint, defined as all cells containing any type of urban land use in NLCD, as well as any additional cells for which NLCD has no urban area but NUDAPT urban fraction (buildings + roads) is greater than 0.3.

2.2. Evaluation of Model Simulations

2.2.1. MODIS

Three methods for comparing MODIS LST to HRLDAS T_{rad} are evaluated in *Hu et al.* [2014], and the optimal technique is employed for the analysis in the present study. The reader is referred to *Hu et al.* [2014] for a more thorough description of, and justification for, the data and methodology than is presented here. The MODIS sensor on board the Terra and Aqua satellites provides global coverage of LST four times daily. The spatial resolution is as high as 1 km for LST, which coincides with the scale of the HRLDAS output. The LST MOD11A1 (Terra) and MYD11A1 (Aqua) Version 5 [*Wan*, 2008] products from 2003 to 2012 summers (June-July-August, JJA) across the Houston area are collected and processed. The median local standard times of satellite overpasses for the data sets are about 11:16 (Terra day), 13:34 (Aqua day), 22:34 (Terra night), and 02:16 (Aqua night). Therefore, 11:30, 13:30, 22:30, and 02:30 are selected as the four daily local standard times to compare HRLDAS with MODIS, because these are the nearest half hours to the median MODIS overpass times. Cloudy pixels are removed in MOD11A1 and MYD11A1 Version 5 [*Wan*, 2008], which is an especially important consideration over Houston, where daytime clouds occur frequently [*Burian and Shepherd*, 2005]. Additionally, because numerous cloud-contaminated pixels are still found within the data, manifested as LST outliers, only MODIS LST data within 1.5 times the interquartile range are used. Finally, only passes between −35° and +35° from nadir are used in order to minimize view-angle biased MODIS LSTs, which are most apparent for larger view angles (view angles range from −65° to +65° from nadir). All remaining MODIS LST pixels after applying these masks for clouds and view angles are used for the comparison with HRLDAS T_{rad}. The MODIS LST data therefore represent clear-sky conditions.

The HRLDAS T_{rad} data are sampled conditionally based upon the remaining MODIS LST data, i.e., on a pixel-by-pixel basis. For example, if there are 103 available MODIS pixels for grid cell *X* spread across the total 920 days (10 years times 92 d/yr), those same 103 grid cells are selected from HRLDAS for the comparison. This approach thus assumes the cloud distributions in MODIS and HRLDAS are similar in time and space (clouds are not explicitly resolved in the HRLDAS forcing data, so determining whether they are present at a

given simulated time is not directly possible), which *Hu et al.* [2014] demonstrate to be a reasonable assumption. The approach has the advantages of using the largest possible sample size for the comparison and being temporally consistent between both data sets. It has the disadvantages of having unequal sample sizes from each grid box, and the possibility of unaccounted for cloud influences in the HRLDAS simulations. The total sampled pixels for 2003–2012 is about 16.8%, 11.6%, 24.2%, and 20.7% of the total possible pixel days in the domain (excepting water areas) for Terra day, Aqua day, Terra night, and Aqua night passes, respectively. Therefore, even the smallest sample of 11.6% yields, a robust sample of 1,550,428 available grid cells over the 125×125 cell domain (less 1097 water grid points) for the 920 day period, which is adequate to draw statistically meaningful conclusions. The analysis herein focuses on the three urban types: light-intensity urban, heavy-intensity urban, and commercial/industrial urban, as well as a variety of vegetation types. Due to the major focus on urban regions, in the few instances where rural areas are analyzed, all vegetation types are combined for the analysis.

### 2.2.2. Screen-Height Air Temperature and Humidity Observations

HRLDAS T_{air} data are compared for the month of August 2006 to hourly screen-height air temperature measurements from a dense network of 17 weather stations (Figure 1) installed for the Second Texas Air Quality Experiment (TEXAQS-II) [*Parrish et al.*, 2009]. HRLDAS data are bilinearly interpolated to the location of each weather station. The data are then averaged across stations by hour to facilitate analysis and comparison of the diurnal cycle among the observations and eight experiments.

3. Results

3.1. Distribution Comparison of MODIS LST and HRLDAS T_{rad}

The probability distributions of MODIS LST and HRLDAS T_{rad} are compared for JJA 2003–2012 for each experiment (EXP), overpass, and urban land use type (Figure 2). As expected, HRLDAS T_{rad} becomes progressively warmer by changing from an urban surface with vegetation only (EXPs A), to one with a light-intensity urban land use type (EXPs B), to one with three urban land use types of increasing intensity (EXPs C). The mean HRLDAS T_{rad} decreases from EXPs C to EXPs D because the use of NUDAPT for EXPs D yields substantially less fractional urban area (i.e., more vegetation) per pixel. The mean NUDAPT urban fractions for light-intensity, heavy-intensity, and commercial/industrial urban land use types in EXPs D are about 0.17, 0.27, and 0.41, compared with 0.50, 0.90, and 0.95 as the default values in EXPs C. Substantial warm biases exist across most experiments and land use types during daytime (up to about 8.6 K for the average of EXPs C1), tending to be greatest for the light-intensity urban category compared to the heavy-intensity and commercial/industrial categories. This seemingly paradoxical relationship can be attributed to a warm bias over the vegetated fraction of each pixel, which can be detected by examining the vegetation-only simulations (EXPs A). In general, for a given pixel consisting of both vegetation and urban components one would expect T_{rad} for vegetation to be cooler than MODIS LST, and T_{rad} for urban surfaces to be warmer, so that the weighted average of the two (if the model were perfect) would be equal to MODIS LST, which measures the combined vegetation + urban radiative temperature for each pixel. This bias is most prominent for light-intensity urban pixels because they have the largest vegetated fraction. A sensitivity experiment in which the vegetation type within urban areas is changed from the default savanna to forest (not shown) does little to reduce the T_{rad} bias because the skin temperature of the forested vegetation is no cooler than for the grassy savanna. Adding irrigation reduces the T_{rad} biases (EXPs A2-D2, green distributions in Figure 2) because more energy is partitioned toward the latent heat fluxes (evapotranspiration) rather than sensible heat fluxes over the vegetated portion of pixels. For example, the root-mean-square error (RMSE) of T_{rad} is reduced (because the bias is reduced) on average by about 39% during daytime for EXP A2 versus EXP A1. However, the vegetation-only T_{rad} (EXP A2) is still warmer on average than MODIS LST for all Terra day experiments and the light-intensity Aqua day experiment. While a full analysis of the causality of the warm bias of HRLDAS T_{rad} for vegetated surfaces is beyond the scope of the present work, it is partly due to an apparent warm bias in the NLDAS-2 temperatures used to force the HRLDAS simulations (discussed in section 3.4).

HRLDAS T_{rad} biases are much smaller at nighttime compared to daytime, partly because biases between latent and sensible heat flux partitioning are not as pronounced in the absence of solar forcing. HRLDAS T_{rad} for the vegetation-only scenarios (EXPs A) is cooler than MODIS LST, as expected. The comparative impacts of altering the number of urban types (EXPs B versus EXPs C) versus adjusting urban fraction (EXPs C versus EXPs D)
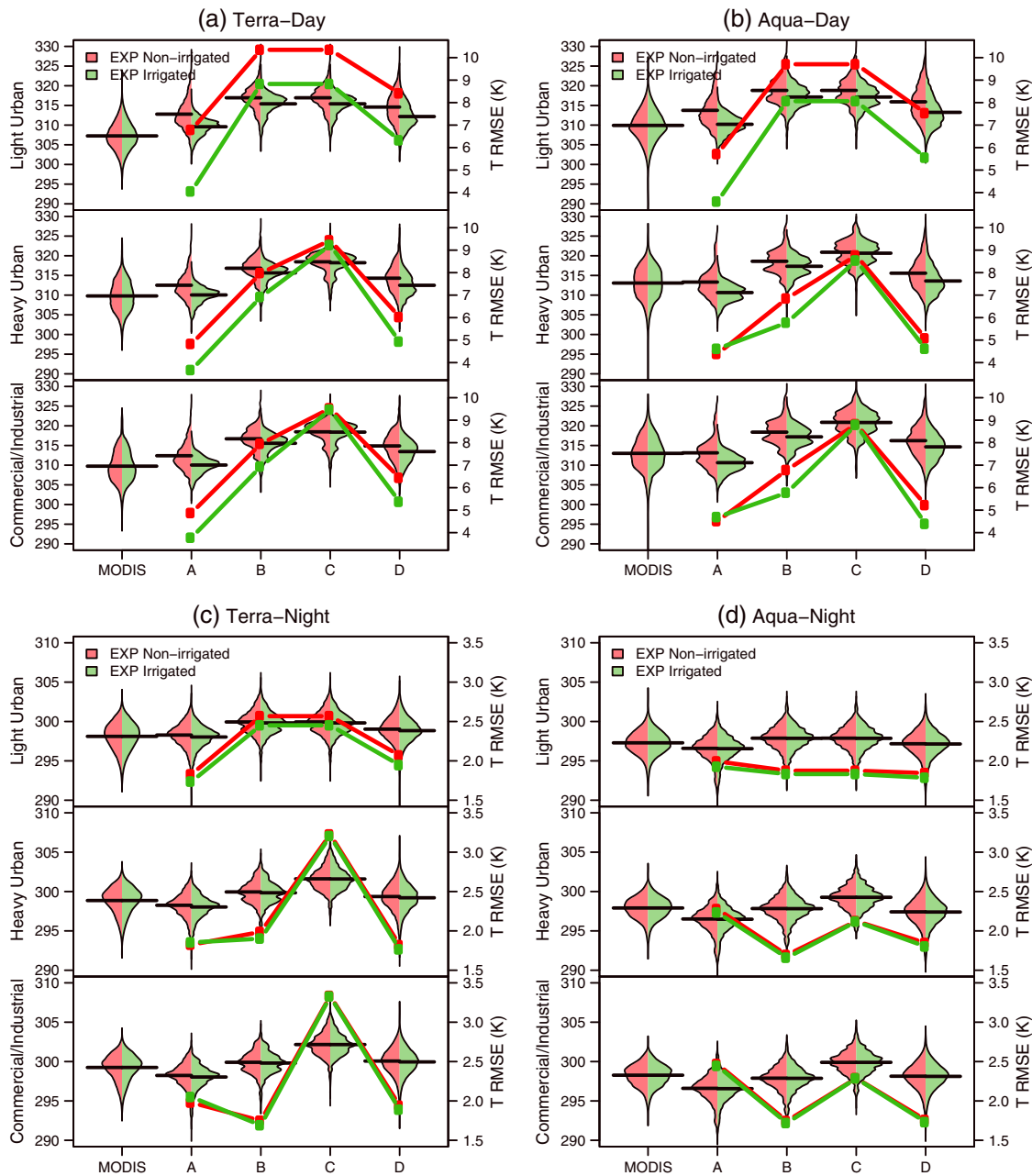
Figure 2. Comparison of 2003–2012 JJA distributions of MODIS LST with HRLDAS T_{rad} (K; left axis) for Terra and Aqua (a, b) daytime and (c, d) nighttime passes. Scenarios are grouped by nonirrigated (A1–D1; red) and irrigated (A2–D2; green) experiments, as well as by (top) light-intensity, (middle) heavy-intensity, and (bottom) commercial/industrial-intensity urban land use types. MODIS LST distributions are identical for both groups of scenarios. The black bars represent mean values. The root-mean-square errors (RMSEs) between MODIS and each HRLDAS scenario are shown with the red (nonirrigated) and green (irrigated) lines (K; right axis).

are almost equivalent, while the irrigation impact is trivial (EXPs A2-D2 versus EXPs A1-D1) because evapotranspiration is negligible. It is evident from Figure 2 that a portion of the RMSE is attributed to the HRLDAS T_{rad} warm bias compared to MODIS LST.

In order to better understand the experimental results in the context of biased and unbiased errors, the systematic (RMSE_s) and unsystematic (RMSE_u) components of RMSE [*Willmott et al.*, 1985] are calculated at each time of day and for the three urban types. RMSE_s is a measure of the modeled linear bias, and RMSE_u is a measure of model precision. Noting that MSE = RMSE² and that RMSE² = RMSE_s² + RMSE_u², the proportions of MSE_s and MSE_u to MSE are calculated (Figure 3). The MSE_s proportion pattern is consistent
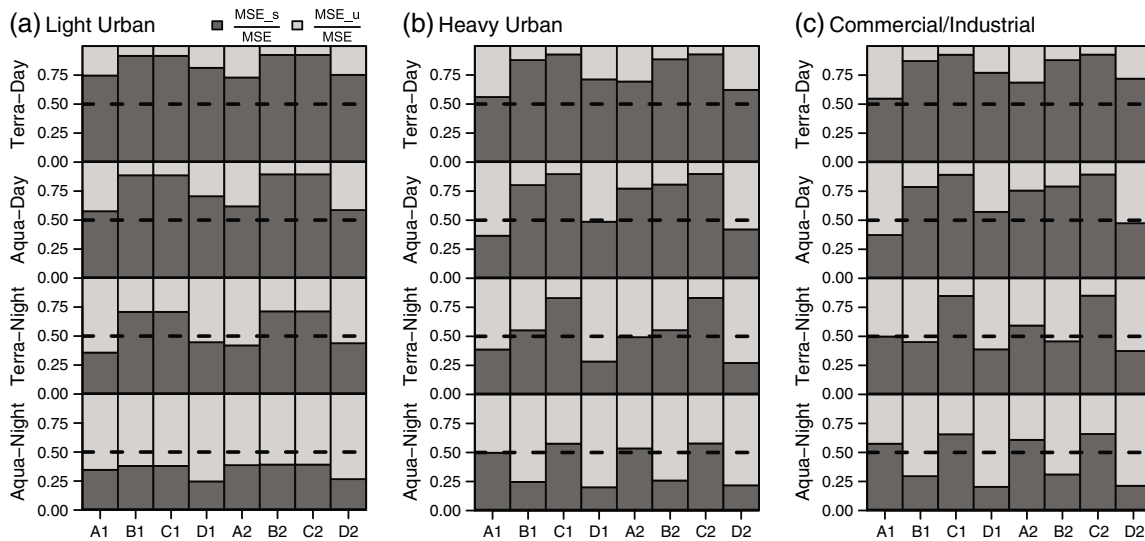
Figure 3. The ratio of systematic mean square error (MSE_s; dark grey) and unsystematic mean square error (MSE_u; light grey) to mean square error (MSE). MSE_s + MSE_u = MSE. The dark dash line is at 0.5, where MSE_s and MSE_u are equal. Scenarios are grouped by (a) light-intensity, (b) heavy-intensity, and (c) commercial/industrial-intensity urban land use types, as well as by the satellite and overpass time.

with the biases in Figure 2, with MSE_s being the major component of total MSE during daytime when large biases occur, whereas MSE_u is generally the largest component during nighttime when biases are small. Interestingly, the proportions remain approximately the same for the non-irrigated (EXPs A1-D1) versus irrigated (EXPs A2-D2) simulations, despite overall lower RMSEs for the irrigated experiments, indicating that irrigation not only reduces the bias but also improves model precision. Although EXP A2 (vegetated only) has comparatively low RMSEs and biases, especially during daytime and for light-urban land use types, EXP D2 generally exhibits the lowest RMSEs (Figure 2) and lowest MSE_s (Figure 3) among those experiments that contain urban land use types (EXPs B, C, and D) during both daytime and nighttime.

To assess the primary drivers of HRLDAS T_{rad}, the distributions of the component radiative temperatures for JJA 2003–2012 are analyzed for EXPs D1 and D2 (Figure 4). The three urban surfaces that contribute to T_{rad_U} —T_{roof}, T_{road}, and T_{wall}—vary substantially during daytime hours, with T_{road} being about 8.1 K (Terra day) and 10.7 K (Aqua day) warmer than T_{roof}, and about 6.8 K (Terra and Aqua day) warmer than T_{wall}, a result that is nearly identical for all three urban types. During night, the urban component temperatures cool by 20–30 K for the Aqua overpass time (13–25 K for Terra), with T_{road} cooling the most, making it on average about 2.1 K warmer than T_{roof} and 1.6 K cooler than T_{wall}. The differential cooling of these three components is due to the nighttime surface energy balance, which becomes dominated by sensible heat and long-wave radiative losses that are proportional to the magnitude T_{rad} reaches during daytime (i.e., the largest losses occur for T_{road}). Within the canyon there are exchanges of sensible and radiative heat between the road and walls, causing the walls to cool at a slower rate than the (initially warmer) road. Interestingly, the integrated urban radiative temperature, T_{rad_U}, is warmer for the light-intensity urban type during daytime than for heavy-intensity and commercial/industrial types, because T_{road} is greater in light-intensity areas due to less shading from shorter buildings (average building heights are 5.0 m, 7.5 m, and 10.0 m for light, heavy, and commercial/industrial intensity, respectively). By contrast, at nighttime the commercial/industrial-intensity urban type is about 0.4–0.5 K and 0.8–0.9 K warmer than heavy- and light-intensity urban types for Terra and Aqua respectively, because T_{wall} and T_{road} do not cool as much among taller buildings due to trapped heat in the urban canyon. The mean radiative temperature for vegetation, T_{rad_V}, is similar among all daytime and all nighttime scenarios. Irrigation decreases the vegetation temperature by about 3.4 K, 2.6 K, and 2.4 K for light-, heavy-, and commercial/industrial-intensity land use types, respectively, during daytime compared to both Terra and Aqua and has a nearly negligible impact during nighttime. Irrigation has no impact on any of the urban radiative temperature components, because the UCM assumes there is no latent heat flux over urban areas. Thus, when T_{rad_V} and T_{rad_U} are combined to calculate T_{rad}, the impact of irrigation is smaller than for T_{rad_V} alone, about 2.5 K, 1.9 K, and 1.5 K for the three respective urban types. Interestingly, mean daytime
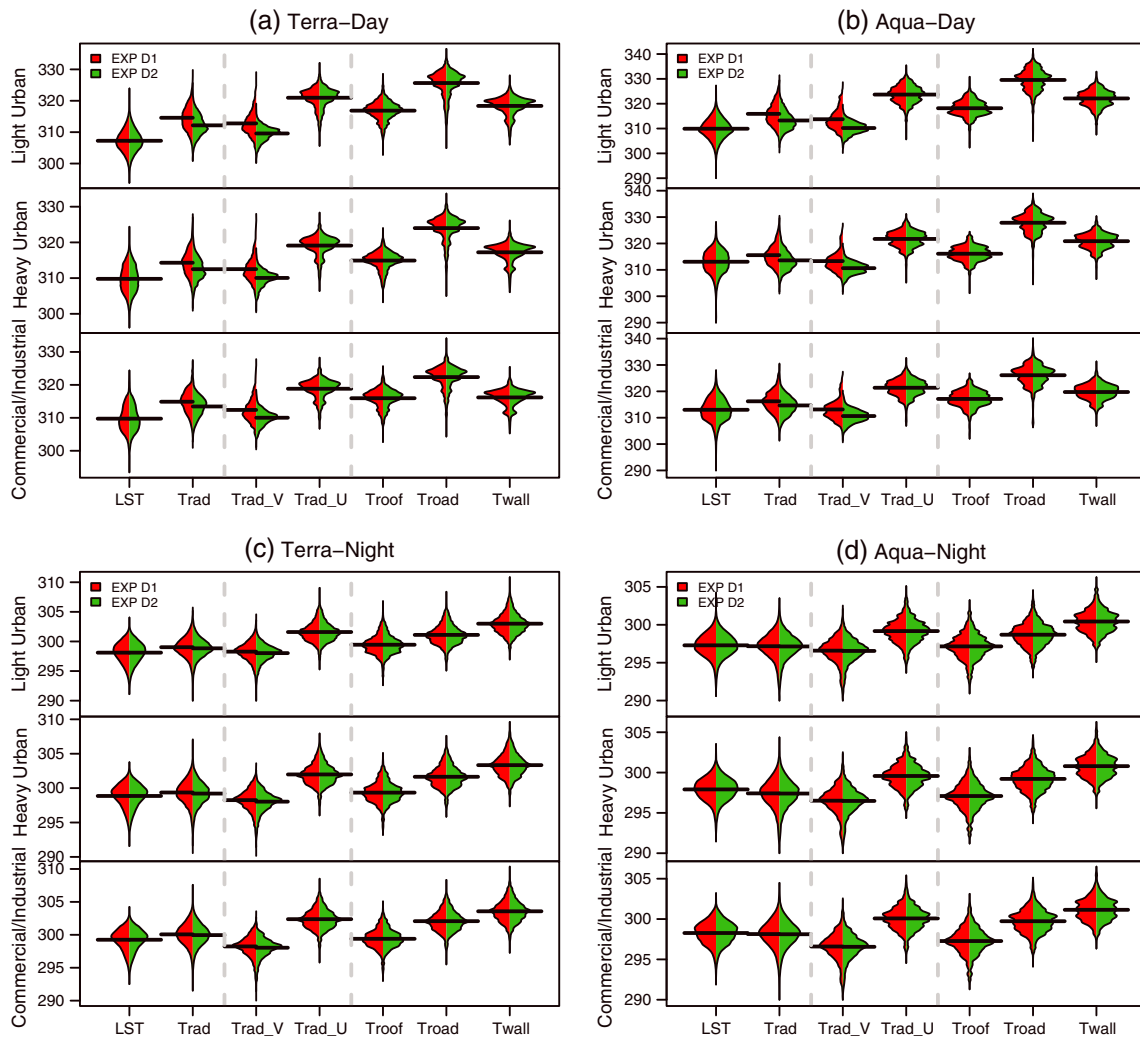
Figure 4. Comparison of the 2003–2012 JJA distributions of MODIS LST with the components of HRLDAS T_{rad} (K; left axis) for Terra and Aqua (a, b) daytime and (c, d) nighttime passes. Scenarios are grouped by experiment D1 (red) and D2 (green), as well as by (top) light-intensity, (middle) heavy-intensity, and (bottom) commercial/industrial-intensity land use types. The component temperatures for HRLDAS T_{rad} (T_{rad_V}, T_{rad_U}, T_{roof}, T_{road}, and T_{wall}) are described in the methods section. The black bars represent mean values.

HRLDAS T_{rad} differs among the three urban types by less than 1 K (commercial/industrial areas are warmest), which is a smaller difference than for MODIS LST, which differs by about 2.5–3.0 K among urban types. The similarity of HRLDAS T_{rad} among the three urban types is caused by the compensating effect of warmer road temperatures for light-intensity urban pixels compared to more urban fraction for heavy- and commercial/industrial-intensity pixels. Both HRLDAS T_{rad} and MODIS LST differ by about 1 K among the three urban types at nighttime.

3.2. Spatial Comparison of MODIS LST and HRLDAS T_{rad}

HRLDAS T_{rad} from EXPs C2 and D2 is compared with MODIS LST spatially for the 2003–2012 JJA average of all available Terra daytime, nighttime, and diurnal data for each pixel (Figure 5). Results are similar for Aqua (not shown). Because averages are performed independently for each pixel, the maps are not temporally congruent in space (e.g., far more days are available for the less cloudy rural areas than the cloudier urban core). Diurnal maps were calculated from the differences of the averaged day and night radiative temperature maps. The urban heat island is evident in both HRLDAS T_{rad} and MODIS LST. It is noteworthy that the urban-to-rural temperature difference is larger during the daytime than the nighttime and that the diurnal cycle is larger in the urban core than in the outlying rural areas. Both phenomena are somewhat
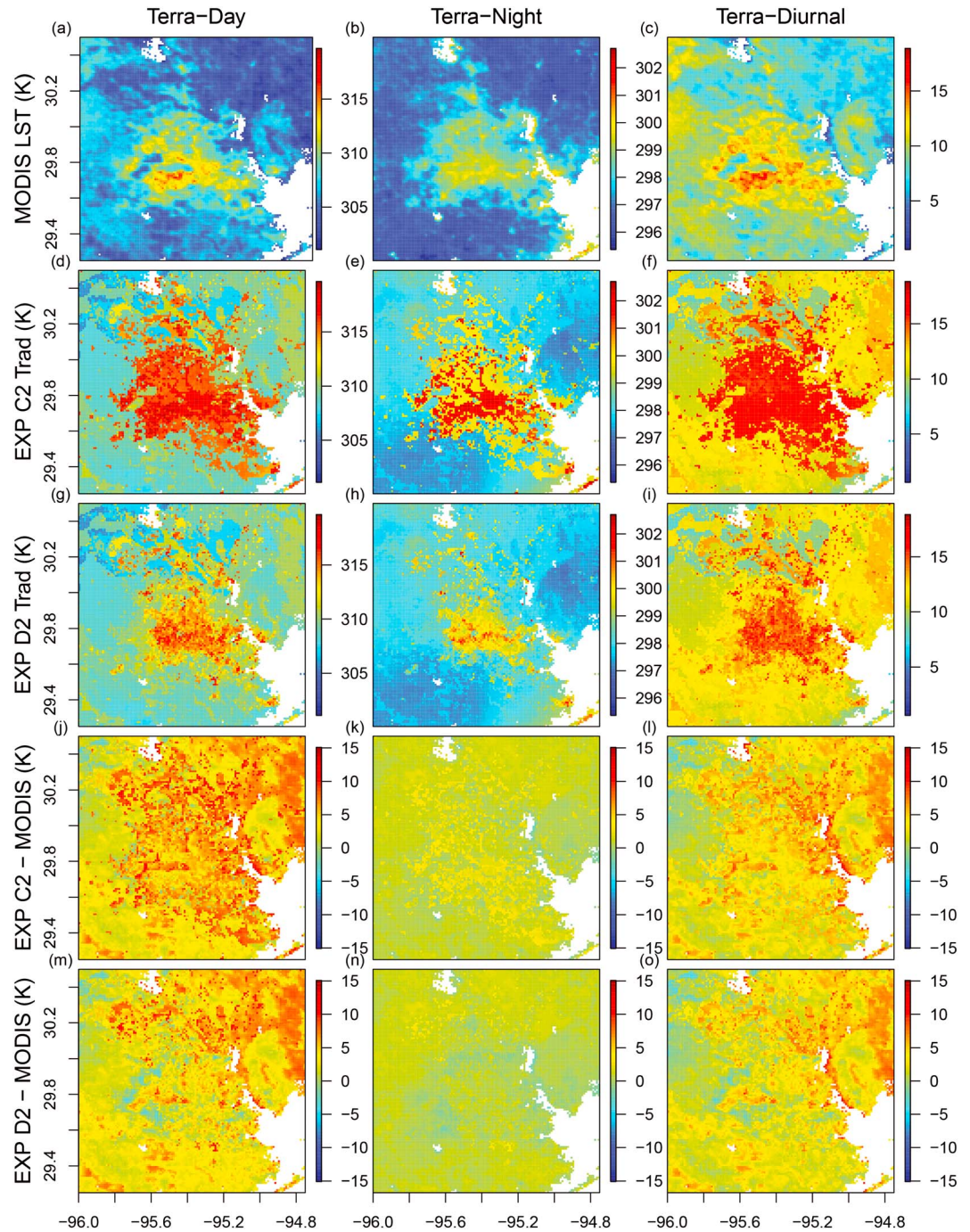
Figure 5. The 2003–2012 average JJA (row 1) MODIS LST (Terra) and (rows 2 and 3) HRLDAS T_{rad} for experiments C2 and D2, for (column 1) day, (column 2) night, and (column 3) difference of day and night (diurnal). (rows 4 and 5) The difference maps for HRLDAS minus MODIS for experiments C2 and D2 are shown.

counterintuitive to the convention for urban heat islands, which typically have larger urban-to-rural differences at nighttime, and which have smaller diurnal cycles over the urban core compared to outlying areas due to the larger thermal inertia of the built environment [e.g., *Oke*, 1982]. The paradox is caused by the use of radiative temperature, rather than air temperature, for the present analysis. Radiative temperature undergoes larger fluctuations over urban regions than rural regions because urban surface energy fluxes have larger swings compared to rural areas due to differences in surface properties [*Roth et al.*, 1989].
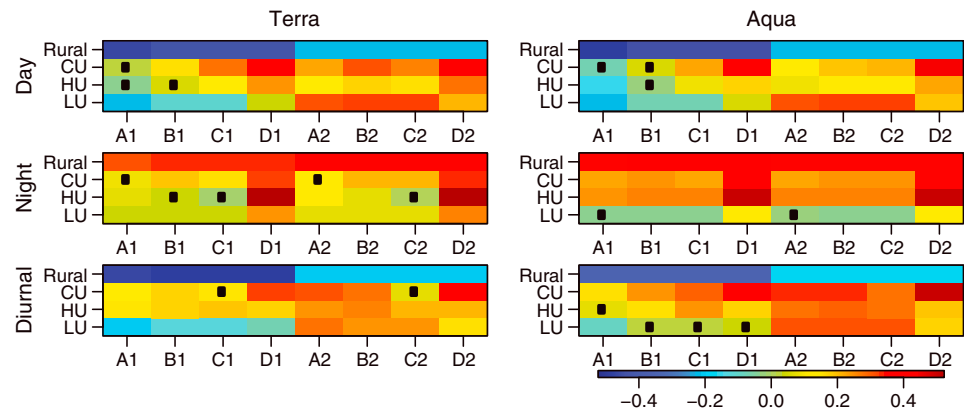
Figure 6. The Pearson's pattern correlation coefficient between the 2003 and 2012 average JJA MODIS LST for (left column) Terra and (right column) Aqua and HRLDAS T_{rad} (experiments C2 and D2) for (top row) day, (middle row) night, and (bottom row) difference of day and night (diurnal). Scenarios are grouped by land use type (rural vegetation = rural, commercial/industrial-intensity urban = CU, heavy-intensity urban = HU, light-intensity urban = LU). Black squares indicate statistical *insignificance* ($p < 0.05$). Note that "Rural" in Figures 6–8 refers to all pixels of any vegetation type that lie outside of urban pixels.

Differences between HRLDAS T_{rad} and MODIS LST are apparent for both day and night, and for both rural and urban pixels. For example, a daytime HRLDAS T_{rad} warm bias in the northeast corner of the domain (outside of Greater Houston) is strongly related to vegetation types; shrubland (about 2% of nonwater pixels) and wooded wetland (about 23% of nonwater pixels) vegetation types in this area have T_{rad} biases of about 7 K and 5 K, respectively, suggesting the specified properties and/or surface types themselves may require refinement. Within the urban area, large HRLDAS warm biases are prevalent during daytime in EXP C2. Irrigation (EXP D2) greatly reduces and in some cases reverses the HRLDAS daytime warm bias over Greater Houston. At nighttime HRLDAS biases are comparatively smaller, and the bias patterns are more homogeneous. The HRLDAS T_{rad} diurnal range is generally overestimated, mainly due to the simulated warm bias during daytime. Greater spatial heterogeneity is evident in MODIS LST within the urban areas compared to HRLDAS T_{rad}, likely due to unavoidable simplifications in the model regarding assumed subgrid-scale features and parameter estimates.

The spatial pattern correlation coefficients between HRLDAS T_{rad} and MODIS LST are estimated for all experiments (Figure 6), based on the 2003–2012 JJA average temperature maps (like those shown in Figure 5). The results quantify some of the qualitative conclusions drawn from inspection of Figure 5. HRLDAS T_{rad} is correlated more strongly with MODIS LST at nighttime compared to daytime. Generally, correlations become stronger with progressively better representation of the urban surface but especially for EXPs D1 and D2 compared to A1–C1 and A2–C2, respectively. Thus, the inclusion of explicit urban fraction generates the largest increases in correlation coefficients. The improvement is most consistent for the commercial/industrial-intensity urban types during daytime, and all urban types at nighttime. Irrigation (EXPs A2–D2) improves the pattern correlations during daytime, a result that is consistent with the finding in section 3.1 that irrigation not only reduces biases but also improves precision. Diurnal correlation coefficients are similar to those for daytime, emphasizing the dominance of HRLDAS T_{rad} daytime errors on errors in the diurnal cycle. Finally, while correlations between HRLDAS T_{rad} and MODIS LST over rural vegetated surfaces are comparatively high during nighttime, they are anticorrelated during daytime, even for the irrigated experiments. The results from this subsection suggest that future work to improve the representation of vegetation in land surface models may yield substantial gains in model accuracy, in both urban and rural areas.

3.3. Temporal Comparison of MODIS LST and HRLDAS T_{rad}

Assessing the interannual variability of urban temperatures provides a collective measure of how well the HRLDAS simulates the frequency, magnitude, and intensity of urban extremes from year to year. The interannual variability of HRLDAS T_{rad} and MODIS LST, along with the NLDAS-2 forcing temperature and
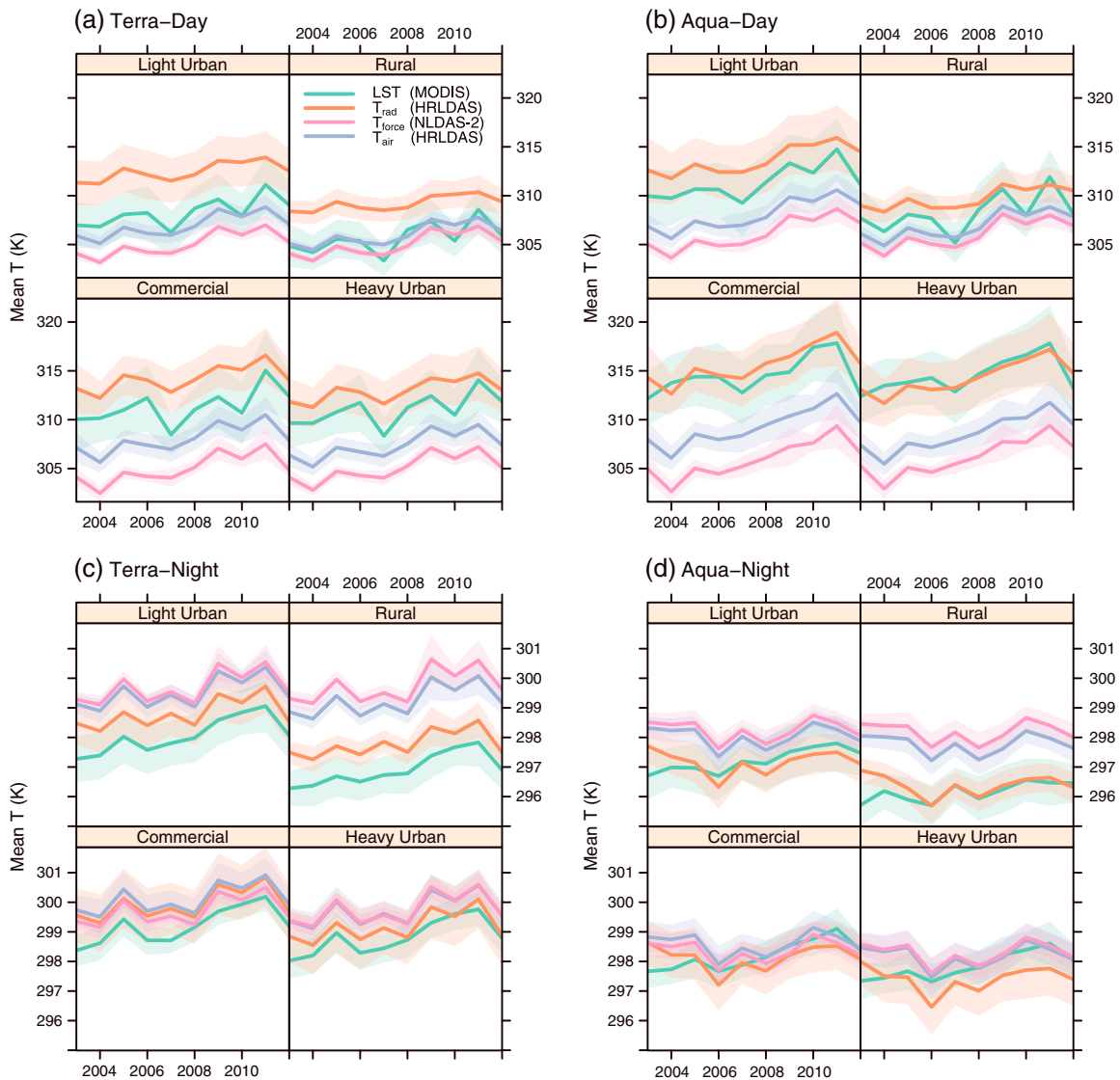
Figure 7. The 2003–2012 domain average, annual average JJA temperatures for four surface types for MODIS LST, HRLDAS T_{rad}, NLDAS-2 T_{force}, and HRLDAS T_{air} for Terra and Aqua (a, b) daytime and (c, d) nighttime passes. HRLDAS results are from experiment D2. The shaded areas indicate ±1 standard deviation from the 10 year average for each land cover type.

HRLDAS T_{air}, is compared for JJA 2003–2012 for EXP D2 (Figure 7). MODIS LST exhibits comparatively large (small) interannual variations for daytime (nighttime). Correlations between the HRLDAS T_{rad} and MODIS LST time series are generally >0.80 for daytime and nighttime (Table 3), except for Aqua nighttime, when there is disagreement during the beginning of the time series that lowers the correlations. However, the nighttime correlations may be sensitive to small errors because the interannual variations are smaller; for example, the RMSE between nighttime HRLDAS T_{rad} and MODIS LST is only 0.8 K and 0.4 K for Terra and Aqua, respectively, for the light-intensity urban type. The interannual variability of daytime HRLDAS T_{rad} tends to be underestimated compared to MODIS LST, whereas nighttime interannual variability is similar or larger than for MODIS (Figure 7 and Table 4). The dampened (amplified) HRLDAS T_{rad} during daytime (nighttime) appears to be related to the NLDAS-2 forcing temperature, to which T_{rad} exhibits similar variability. In general, increasing temporal trends of similar magnitude are present in all time series (Table 4). However, statistically *insignificant* positive trends are apparent for most of the MODIS LST daytime series, whereas all of the HRLDAS T_{rad} daytime trends are significant ($p < 0.05$) because of their comparatively dampened variability. Conversely, the nighttime MODIS LST trends are all statistically

Table 3. The Pearson's Correlation Coefficients Between the Domain Average, Annual Average JJA 2003–2012 MODIS LST and HRLDAS T_{rad} (Experiment D2) for Each Land Cover Type for Day, Night, and the Difference Between Day and Night (Diurnal)

	Terra			Aqua		
Land Use	Day	Night	Diurnal	Day	Night	Diurnal
Light-intensity urban	0.83	0.89	0.64	0.92	0.36[a]	0.85
Heavy-intensity urban	0.81	0.89	0.68	0.81	0.43[a]	0.68
Commercial/industrial urban	0.84	0.88	0.72	0.85	0.38[a]	0.78
Rural vegetation	0.75	0.90	0.50[a]	0.80	0.36[a]	0.71

[a]The result is not significant at the 95% confidence interval.

significant, whereas none of the HRLDAS T_{rad} trends are (mainly because the HRLDAS trends are comparatively smaller, although greater variability also plays a role).

To gain a better understanding of the interannual variability at the subdomain scale, distributions of 2003–2012 annual average JJA correlation coefficients and biases between HRLDAS T_{rad} and MODIS LST were calculated for each land use type, satellite, and time of day for EXP D2 (Figure 8). Average pixel correlation coefficients typically range from 0.3 to 0.6 for both day and night. Mean biases are larger during daytime than nighttime, consistent with the spatial results presented above. Relationships are similar among different land use types. Interestingly, daytime correlations are higher for Aqua (afternoon) compared to Terra (before noon), and conversely during nighttime they are higher for Terra (before midnight) and Aqua (after midnight). It is possible that the correlations are highest during the afternoon and evening hours because the surface is more closely coupled to the overlying atmosphere compared to early and late morning hours. Although such coupling is not explicitly captured in the offline HRLDAS simulations, land surface temperatures are likely more similar to overlying air temperatures when coupling is vigorous, and therefore our simulations, which are partially a function of the NLDAS-2 air temperatures used to force them, may be more accurate. In summary, the temporal analysis indicates that for EXP D2, the most realistic scenario, T_{rad} is more accurate at night than during day and generally has the highest correlations during the afternoon and late evening.

3.4. Comparison of Meteorological Observations and HRLDAS T_{air}

Comparing HRLDAS T_{rad} to MODIS LST provides a means to comprehensively examine model performance spatially over a long period. It is also useful to compare HRLDAS T_{air} to air temperature observations from weather stations if available, as air temperature is often the variable of interest for assessing extreme heat events. HRLDAS T_{air} data are compared for the month of August 2006 to hourly screen-height air temperature measurements (Figure 9), with the results averaged across 17 weather stations (shown in Figure 1) for the

Table 4. The Standard Deviation After Detrending the 2003–2012 Domain Average, Annual Average JJA MODIS LST, HRLDAS T_{rad} (Experiment D2), and NLDAS-2 T_{force}, for Each Land Cover Type, Satellite, and Time of Day (Top)[a]

|	Light-Intensity Urban			Heavy-Intensity Urban			Commercial/Industrial Urban			Rural Vegetation		
Pass	LST	T_{rad}	T_{force}	LST	T_{rad}	T_{force}	LST	T_{rad}	T_{force}	LST	T_{rad}	T_{force}
						Standard Deviation After Detrending (K)						
Terra day	1.04	0.67	0.81	1.28	0.82	0.96	1.44	0.99	1.06	1.23	0.51	0.77
Aqua day	1.25	0.81	0.85	1.39	0.93	1.01	1.68	1.17	1.09	1.64	0.65	0.89
Terra night	0.37	0.42	0.46	0.4	0.43	0.45	0.41	0.44	0.42	0.32	0.36	0.47
Aqua night	0.19	0.4	0.35	0.24	0.43	0.37	0.28	0.43	0.36	0.21	0.35	0.34
						Trend (K yr^{-1})						
Terra day	0.33	0.23	0.31	0.33[b]	0.27	0.34	0.34[b]	0.28	0.35	0.29[b]	0.19	0.31
Aqua day	0.39	0.39	0.45	0.36[b]	0.46	0.52	0.30[b]	0.47	0.51	0.33[b]	0.28	0.38
Terra night	0.16	0.09[b]	0.10[b]	0.15	0.09[b]	0.09[b]	0.15	0.10[b]	0.08[b]	0.14	0.08[b]	0.11[b]
Aqua night	0.11	0.00[b]	-0.01[b]	0.13	0.00[b]	0.00[b]	0.14	0.01[b]	0.00[b]	0.08	-0.01[b]	-0.01[b]

[a]The 2003–2012 trends (bottom).
[b]The result is not significant at the 95% confidence interval.
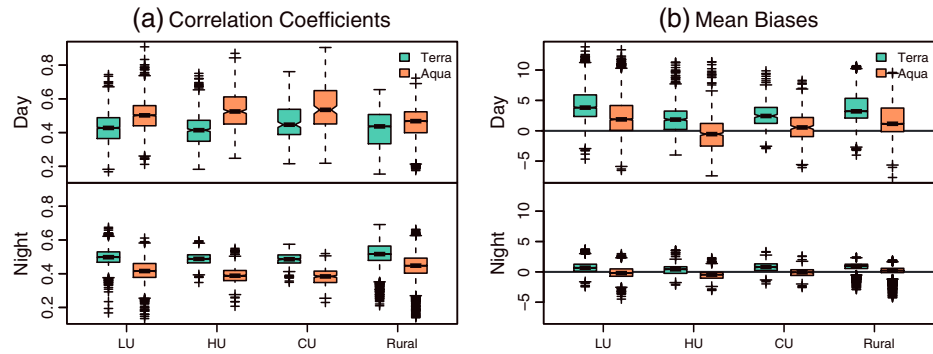
Figure 8. Box plots of the Pearson's temporal correlation coefficients and mean biases (K) for HRLDAS T_{rad} (experiment D2) versus MODIS LST. Metrics are calculated for the 2003–2012 annual average JJA time series at each pixel and placed into distributions by land use type and time of day. Pixels with insignificant correlations ($p < 0.05$) are excluded. Colored regions indicate the interquartile range.

monthly mean diurnal cycle. HRLDAS T_{air} for all experiments is warmer than observed during the daytime hours (~0800–2100 LST), and cooler than observed during nighttime. As with the results for T_{rad} presented above, daytime T_{air} biases are smallest (but still positive) for the vegetation-only experiment (EXP A1), largest for the three-class urban experiment with fixed urban fraction (EXP C1), and are reduced when NUDAPT is employed to explicitly specify urban fraction (EXPs D1 and D2). While the daytime warm bias (1–3 K) for T_{air} is not surprising given its consistency with the T_{rad} comparison with MODIS LST, the nighttime cool bias (0.25–1.25 K) for T_{air} is more prominent than for T_{rad}, which is generally unbiased or slightly warmer than MODIS LST (e.g., Figure 2). These opposing daytime and nighttime biases result in the diurnal cycle of T_{air} being larger than observed by about 1–5 K, mainly due to the daytime warm bias. The daytime warm bias is partly due to the forcing temperature, because NLDAS-2 T_{force} is approximately the same as or slightly warmer than the observed air temperature, and T_{air} and T_{rad} cannot be cooler than T_{force} during daytime hours unless a temperature inversion exists (which is extremely unlikely during summer in Houston). However, the amplitude of the diurnal cycle for T_{force} is approximately the same as observed, so it likely contributes little to the overestimated diurnal cycle of HRLDAS T_{air}. The larger-than-observed diurnal cycle of T_{air} in the HRLDAS simulations may be partly related to the simulations being performed offline with no
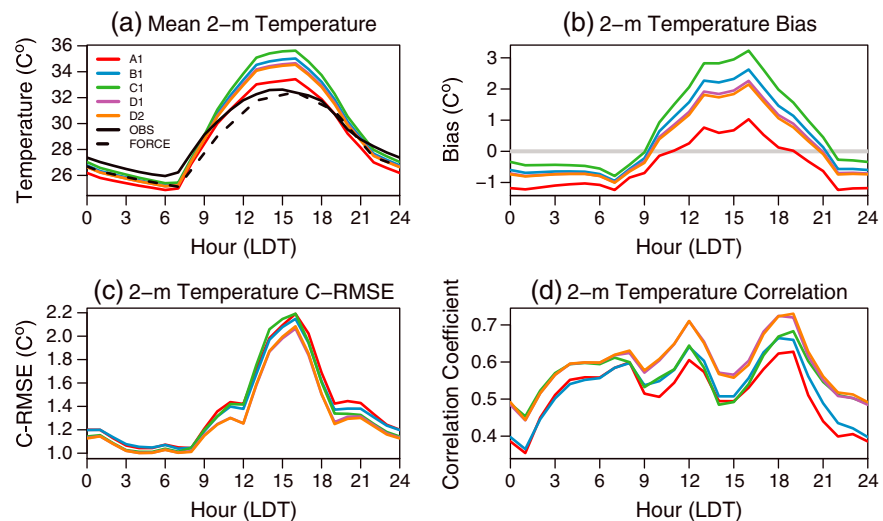
Figure 9. (a) Comparison of the August 2006 average diurnal cycle of 2 m air temperature (T_{air}) for five HRLDAS experiments (A1, B1, C1, D1, and D2) with screen-height air temperature from the TEXAQS-II weather stations (OBS) and the variable-height NLDAS-2 forcing data used to drive HRLDAS (FORCE). (b–d) The bias, C-RMSE, and Pearson's correlation coefficient, respectively, for each of the five HRLDAS experiments versus OBS. The grey line in Figure 9b indicates a bias of zero.

coupling present between the surface and atmosphere. Such coupling might otherwise dampen the HRLDAS daytime warm bias (e.g., via a wind speed feedbacks related to afternoon sea breezes).

The centered RMSE (C-RMSE), which is a measure of unbiased model error versus observations (much like the RMSE_u statistic presented above for T_{rad}), indicates that the model accuracy is highest for EXPs D1 and D2 throughout the diurnal cycle (Figure 9), which supports the findings above for the comparison of HRLDAS T_{rad} with MODIS LST, that the simulations which use NUDAPT urban fraction have higher fidelity. Additionally, correlation coefficients are highest for EXPs D1 and D2 over the entire diurnal cycle, indicating that these experiments best capture temperature variability in time and space based on the 17 station analysis.

4. Discussion and Conclusions

A series of eight 1 km HRLDAS simulation experiments are performed over Greater Houston to explore the model accuracy gained by progressively increasing the complexity of the urban morphology representation in a UCM. The fidelity of the simulations is assessed via comparison to in situ observations of air temperature and remotely sensed estimates of MODIS LST. HRLDAS T_{rad} and T_{air} become progressively warmer by changing from an urban surface with vegetation only (EXPs A), to one with a light-intensity urban land use type (EXPs B), to one with three urban land use types of increasing intensity (EXPs C). However, HRLDAS T_{rad} decreases when EXPs C are modified for EXPs D so that they explicitly employ observationally based estimates of urban fraction in Greater Houston from NUDAPT rather than fixed urban fractions that are a function of the urban land use type. This modification yields HRLDAS T_{rad} simulations that are cooler (and more similar to observed temperatures) because the average NUDAPT urban fraction in each pixel is much lower than assumed in the HRLDAS default settings: 0.17, 0.27, and 0.41, compared with 0.50, 0.90, and 0.95 for the light-, heavy-, and commercial/industrial-intensity urban types, respectively. In summary, of the experiments that include urban land use types, EXP D2 (which differs from EXP D1 only in that it is irrigated) consistently yields the most accurate results spatially and temporally when compared with MODIS LST and screen-height air temperature observations from a network of weather stations.

Differences between HRLDAS simulated temperatures and observed temperatures are due to myriad factors. Observational constraints lead to some of the differences, despite efforts to reduce their impact. For example, *Hu et al.* [2014] demonstrate that MODIS LST is biased as a function of the view angle of each overpass and that cloud contamination of some pixels still is present even in quality-controlled versions of MODIS data. Additionally, despite efforts to ensure MODIS LST and HRLDAS T_{rad} are consistent, it is not clear that MODIS "sees" from space the same surface that HRLDAS simulates. For example, MODIS may detect a greater fraction of vegetation in many pixels due to trees obscuring buildings. The UCM in HRLDAS does not simulate the effects of vegetation shading on urban surfaces, which may lead to overestimated HRLDAS T_{rad} warm biases compared to MODIS LST. Regardless of the observational constraints, comparisons of HRLDAS T_{rad} and T_{air} with MODIS LST and weather station observations clearly indicate a warm bias in the HRLDAS temperature simulations during daytime. Examples of model constraints that likely contribute to the warm bias include performing the HRLDAS simulations offline (i.e., uncoupled to an atmospheric model) to reduce computational expense, inadequate representation of subgrid-scale processes and land use heterogeneity, and the use of outdated or inaccurate morphological data sets. For example, HRLDAS land use remains static throughout 2003–2012. However, the MODIS MCD12Q1 yearly land cover product indicates rapid changes throughout the period, such as an increase in urban area of 78 km^2 from 2003 to 2005.

In the present study the most accurate urban simulations are yielded from experiments that (1) explicitly specify the urban fraction in each pixel and (2) include irrigation. The former modification (explicit land use) yields a gain in accuracy that is larger than for several other modifications tested, suggesting that continuing to improve urban morphological data sets, as has been done in recent years [e.g., *Burian and Ching*, 2009], is a worthwhile endeavor. The latter modification (irrigation) substantially reduces simulated temperature biases and increases model precision, presumably because watering lawns, parks, etc. is a common activity that is neglected in the current version of HRLDAS. However, the irrigation approach used in the present study— basically assuming all surfaces are irrigated all of the time—is clearly oversimplified, and for parts of the city and outlying rural areas irrigation may lead to improved results for the wrong reason. Quantitative knowledge of the spatiotemporal distribution of irrigation practices is not well constrained and therefore is difficult to simulate accurately. Such information is greatly needed, and additionally, research is also required

to understand how local policies affect irrigation practices and subsequently the urban heat island. For example, considering that extreme heat events often coincide with droughts [e.g., *Fischer et al.*, 2007], what are the trade-offs of implementing urban watering restrictions that likely exacerbate high temperatures? Public health concerns about heat and projected increases in the frequency, duration, and intensity of extreme heat events emphasizes the need for improved characterization of urban environments in meteorological models so that human exposure to heat both within cities and between urban and rural areas can be more accurately differentiated.

References

Arya, S. (1998), *Introduction to Micrometeorology*, Academic Press, New York.

Atwater, M. A. (1972), Thermal effects of urbanization and industrialization in the boundary layer, *Boundary Layer Meteorol.*, *3*, 229–245.

Best, M. J. (2005), Representing urban areas within operational numerical weather prediction models, *Boundary Layer Meteorol.*, *114*, 91–109.

Borden, K. A., and S. L. Cutter (2008), Spatial patterns of natural hazards mortality in the United States, *Int. J. Health Geog.*, *7*, 64, doi:10.1186/1476-072X-7-64.

Bornstein, R., et al. (2006), Modeling effects of land use/land cover modifications on the urban heat island phenomenon and air quality in Houston, Texas, SJSU Final Report to the Houston Advanced Research Center for Project No. R-04-0055, San Jose, Calif.

Burian, S. J., and J. Ching (2009), Development of gridded fields of urban canopy parameters for advanced urban meteorological and air quality models, EPA Rep. EPA/600/R-10/007, Washington, D. C.

Burian, S. J., and J. M. Shepherd (2005), Effect of urbanization on the diurnal rainfall pattern in Houston, *Hydrol. Process.*, *19*, 1089–1103.

Carter, M., J. M. Shepherd, S. Burian, and I. Jeyachandran (2012), Integration of lidar data into a coupled mesoscale-land surface model: A theoretical assessment of sensitivity of urban-coastal mesoscale circulations to urban canopy parameters, *J. Atmos. Oceanic Technol.*, *29*, 328–346, doi:10.1175/2011JTECHA1524.1.

Centers for Disease Control and Prevention (2006), Heat-related deaths—United States, 1999–2003, *Morb. Mortal. Wkly. Rep.*, *55*, 796–798.

Chen, F., and J. Dudhia (2001), Coupling an advanced land surface hydrology model with the Penn State/NCAR MM5 modeling system. Part 1: Model description and implementation, *Mon. Weather Rev.*, *129*, 569–586.

Chen, F., Y. Liu, H. Kusaka, M. Tewari, J.-W. Bao, C.-F. Lo, and K.-H. Lau (2004), Challenge of forecasting urban weather with NWP models, paper presented at 5th MM5 and WRF Users Workshop, National Center for Atmospheric Research, Boulder, Colo.

Chen, F., K. W. Manning, S. B. LeMone, J. G. Alfieri, R. Roberts, M. Tewari, D. Niyogi, and T. W. Horst (2007), Description and evaluation of the characteristics of the NCAR High-Resolution Land Data Assimilation System, *J. Appl. Meteorol.*, *46*, 694–713.

Chen, F., et al. (2011a), The integrated WRF/urban modeling system: Development, evaluation, and applications to urban environmental problems, *Int. J. Climatol.*, *31*, 273–288, doi:10.1002/joc.2158.

Chen, F., S. Miao, M. Tewari, J.-W. Bao, and H. Kusaka (2011b), A numerical study of interactions between surface forcing and sea-breeze circulations and their effects on stagnant winds in the Greater Houston area, *J. Geophys. Res.*, *116*, D12105, doi:10.1029/2010JD015533.

Cheng, F. Y., and D. W. Byun (2008), Application of high resolution land use and land cover data for atmospheric modeling in the Houston-Galveston metropolitan area. Part I: Meteorological simulation results, *Atmos. Environ.*, *42*, 7795–7811.

Ching, J., et al. (2009), National Urban Database and Access Portal Tool, *Bull. Am. Meteorol. Soc.*, *90*, 1157–1168, doi:10.1175/2009BAMS2675.1.

Cosgrove, B. A., et al. (2003), Real-time and retrospective forcing in the North American Land Data Assimilation System (NLDAS) project, *J. Geophys. Res.*, *108*(D22), 8842, doi:10.1029/2002JD003118.

Curriero, F. C., K. S. Heiner, J. M. Samet, S. L. Zeger, L. Strug, and J. A. Patz (2002), Temperature and mortality in 11 cities of the eastern United States, *Am. J. Epidemiol.*, *155*, 80–87.

Dandou, A., M. Tombrou, and N. Soulakellis (2009), The influence of the city of Athens on the evolution of the sea-breeze front, *Boundary Layer Meteorol.*, *13*, 35–51.

Diffenbaugh, N. S., and M. Ashfaq (2010), Intensification of hot extremes in the United States, *Geophys. Res. Letts.*, *37*, L15701, doi:10.1029/2010GL043888.

Duffy, P. B., and C. Tebaldi (2012), Increasing prevalence of extreme summer temperatures in the U.S., *Clim. Change*, *111*, 487–495, doi:10.1007/s10584-012-0396-6.

Fischer, E. M., S. I. Seneviratne, D. Lüthi, and C. Schär (2007), Contribution of land-atmosphere coupling to recent European summer heat waves, *Geophys. Res. Lett.*, *34*, L06707, doi:10.1029/2006GL029068.

Freitas, E. D., C. M. Rozoff, W. R. Cotton, and P. L. Silva Dias (2007), Interactions of an urban heat island and sea-breeze circulations during winter over the metropolitan area of São Paulo, Brazil, *Boundary Layer Meteorol.*, *122*, 43–65.

Greene, S., L. S. Kalkstein, D. M. Mills, and J. Samenow (2011), An examination of climate change on extreme heat events and climate-mortality relationships in large U.S. cities, *Wea. Climate Soc.*, *3*, 281–292, doi:10.1175/WCAS-D-11-00055.1.

Heaton, M. J., et al. (2014), Characterizing urban vulnerability to heat stress using a spatially varying coefficient model, *Spatio-temporal Epidemiol.*, *8*, 23–33, doi:10.1016/j.sste.2014.01.002.

Homer, C. G., C. Huang, L. Yang, B. Wylie, and M. Coan (2004), Development of a 2001 national land-cover database for the United States, *Photogramm. Eng. Remote Sens.*, *70*, 7829–840.

Hu, L., N. A. Brunsell, A. J. Monaghan, M. P. Barlage, and O. V. Wilhelmi (2014), How can we use MODIS land surface temperature to validate long-term urban model simulations?, *J. Geophys. Res. Atmos.*, *119*, 3185–3201, doi:10.1002/2013JD021101.

Jones, T. S., et al. (1982), Morbidity and mortality associated with the July 1980 heat wave in St. Louis and Kansas City, Mo, *J. Am. Med. Assoc.*, *247*, 3327–3331.

Kanda, M., M. Kanega, T. Kawai, R. Moriwaki, and H. Sugawara (2007), Roughness lengths for momentum and heat derived from outdoor urban scale models, *J. Appl. Meteorol. Climatol.*, *46*, 1067–1079, doi:10.1175/JAM2500.1.

Kondo, H., and F. H. Liu (1998), A study on the urban thermal environment obtained through one-dimensional urban canopy model, *J. Jpn. Soc. Atmos. Environ.*, *33*, 179–192.

Kusaka, H., and F. Kimura (2004), Coupling a single-layer urban canopy model with a simple atmospheric model: Impact on urban heat island simulation for an idealized case, *J. Meteorol. Soc. Jpn.*, *82*, 67–80.

Kusaka, H., H. Kondo, Y. Kikegawa, and F. Kimura (2001), A simple single-layer urban canopy model for atmospheric models: Comparison with multi-layer and slab models, *Boundary Layer Meteorol.*, *101*, 329–358.

Kusaka, H., F. Chen, J. W. Bao, and H. Hirakuchi (2004), Simulation of the urban heat island effects over the Greater Houston area with the high resolution WRF/LSM/Urban coupled system, paper presented at Symposium on Planning, Nowcasting, and Forecasting in the Urban Zone, Seattle, Wash.

Kusaka, H., F. Chen, M. Tewari, J. Dudhia, D. O. Gill, M. G. Duda, W. Wang, and Y. Miky (2012a), Numerical simulation of urban heat island effect by the WRF model with 4-km grid increment: An inter-comparison study between the urban canopy model and slab model, *J. Meteorol. Soc. Jpn.*, *90B*, 33–45, doi:10.2151/jmsj.2012-B03.

Kusaka, H., M. Hara, and Y. Takane (2012b), Urban climate projection by the WRF model at 3-km horizontal grid increment: Dynamical downscaling and predicting heat stress in the 2070's August for Tokyo, Osaka and Nagoya metropolies, *J. Meteorol. Soc. Jpn.*, *90B*, 47–63, doi:10.2151/jmsj.2012-B04.

Li, D., and E. Bou-Zeid (2013), Synergistic interactions between urban heat islands and heat waves: The impact in cities is larger than the sum of its parts, *J. Appl. Meteorol. Climatol.*, *52*, 2051–2064, doi:10.1175/JAMC-D-13-02.1.

Masson, V. (2000), A physically-based scheme for the urban energy budget in atmospheric models, *Boundary Layer Meteorol.*, *94*, 357–397.

Medina-Ramon, M., A. Zanobetti, D. P. Cavanagh, and J. Schwartz (2006), Extreme temperatures and mortality: Assessing effect modification by personal characteristics and specific cause of death in a multi-city case only analysis, *Environ. Health Perspect.*, *114*, 1331–1336.

Meehl, G. A., and C. Tebaldi (2004), More intense, more frequent, and longer lasting heat waves in the 21st century, *Science*, *305*, 994–997.

Mesinger, F., et al. (2006), North American Regional Reanalysis, *Bull. Am. Meteorol. Soc.*, *87*, 343–360.

Miao, S., F. Chen, Q. Li, and S. Fan (2011), Impacts of urban processes and urbanization on summer precipitation: A case study of heavy rainfall in Beijing on 1 August 2006, *J. Appl. Meteorol. Climatol.*, *50*, 806–825.

Mills, G. M. (1997), An urban canopy-layer climate model, *Theor. Appl. Climatol.*, *57*, 229–244.

Mitchell, K. E., et al. (2004), The multi-institution North American Land Data Assimilation System (NLDAS): Utilizing multiple GCIP products and partners in a continental distributed hydrological modeling system, *J. Geophys. Res.*, *109*, D07S90, doi:10.1029/2003JD003823.

Oke, T. R. (1982), The energetic basis of the urban heat island, *Q. J. R. Meteorol. Soc.*, *108*, 1–24.

Oke, T. R., G. T. Johnson, D. G. Steyn, and I. D. Watson (1991), Simulation of surface urban heat islands under "ideal" conditions at night. Part 2: Diagnosis of causation, *Boundary Layer Meteorol.*, *56*, 339–358.

Oleson, K. W., A. Monaghan, O. Wilhelmi, M. Barlage, N. Brunsell, J. Feddema, L. Hu, and D. F. Steinhoff (2013), Interactions between urbanization, heat stress, and climate change, *Clim. Change*, doi:10.1007/s10584-013-0936-8.

Otte, T. L., A. Lacser, S. Dupont, and J. K. S. Ching (2004), Implementation of an urban canopy parameterization in a mesoscale meteorological model, *J. Appl. Meteorol.*, *43*, 1648–1665, doi:10.1175/JAM2164.1.

Parrish, D. D., et al. (2009), Overview of the Second Texas Air Quality Study (TexAQS II) and the Gulf of Mexico Atmospheric Composition and Climate Study (GoMACCS), *J. Geophys. Res.*, *114*, D00F13, doi:10.1029/2009JD011842.

Patz, J. A., et al. (2000), The potential health impacts of climate variability and change for the United States: Executive summary of the report of the health sector of the U.S. National Assessment, *Environ. Health Perspect.*, *108*, 367–76.

Patz, J. A., et al. (2005), Impact of regional climate change on human health, *Nature*, *438*, 310–317, doi:10.1038/nature04188.

Roth, M., T. R. Oke, and W. J. Emory (1989), Satellite-derived urban heat islands from three coastal cities and the utilization of such data in urban climatology, *Int. J. Remote Sens.*, *10*, 1699–1720.

Salamanca, F., A. Martilli, M. Tewari, and F. Chen (2011), A study of the urban boundary layer using different urban parameterizations and high-resolution urban canopy parameters with WRF, *J. Appl. Meteorol. Climatol.*, *50*, 1107–1128, doi:10.1175/2010JAMC2538.1.

Schuman, S. H. (1972), Patterns of urban heat-wave deaths and implications for prevention: Data from New York and St. Louis during July 1966, *Environ. Res.*, *5*, 59–75.

Semenza, J. C., C. H. Rubin, K. H. Falter, J. D. Selanikio, W. D. Flanders, H. L. Howe, and J. L. Wilhelm (1996), Heat-related deaths during the July 1995 heat wave in Chicago, *N. Engl. J. Med.*, *335*, 84–90.

Shepherd, J. M., W. M. Carter, M. Manyin, D. Messen, and S. Burian (2010), The impact of urbanization on current and future coastal convection: A case study for Houston, *Environ. Plann.*, *37*, 284–304.

Uejio, C. K., O. V. Wilhelmi, J. S. Golden, D. M. Mills, S. P. Gulino, and J. P. Samenow (2011), Intra-urban societal vulnerability to extreme heat: The role of heat exposure and the built environment, socioeconomics, and neighborhood stability, *Heath Place*, *17*, 498–507.

Vu, T. C., T. Asaeda, and Y. Ashie (1999), Development of a numerical model for the evaluation of the urban thermal environment, *J. Wind Eng. Ind. Aerodyn.*, *81*, 181–191.

Wan, Z. M. (2008), New refinements and validation of the MODIS land-surface temperature/emissivity products, *Remote Sens. Environ.*, *112*, 59–74.

Wilhelmi, O. V., and M. H. Hayden (2010), Connecting people and place: A new framework for reducing urban vulnerability to extreme heat, *Environ. Res. Lett.*, *5*, 014021, doi:10.1088/1748-9326/5/1/014021.

Willmott, C. J., S. G. Ackleson, R. E. Davis, J. J. Feddema, K. M. Klink, D. R. Legates, J. O'Donnell, and C. M. Rowe (1985), Statistics for the evaluation and comparison of models, *J. Geophys. Res.*, *90*, 8995–9005, doi:10.1029/JC090iC05p08995.

Xia, Y., et al. (2012), Continental-scale water and energy flux analysis and validation for the North American Land Data Assimilation System project phase 2 (NLDAS-2): 1. Intercomparison and application of model products, *J. Geophys. Res.*, *117*, D03109, doi:10.1029/2011JD016048.